



Symmetry breaking induced insulating electronic state in $\text{Pb}_9\text{Cu}(\text{PO}_4)_6\text{O}$ Jiaxi Liu,^{1,2,*} Tianye Yu,^{1,*} Jiangxu Li,^{1,†} Jiantao Wang,^{1,2} Junwen Lai,^{1,2} Yan Sun,¹ Xing-Qiu Chen¹ ,¹ and Peitao Liu^{1,‡} ¹Shenyang National Laboratory for Materials Science, Institute of Metal Research, Chinese Academy of Sciences, 110016 Shenyang, China²School of Materials Science and Engineering, University of Science and Technology of China, 110016 Shenyang, China

(Received 19 August 2023; accepted 26 September 2023; published 9 October 2023)

The recent experimental claim of room-temperature ambient-pressure superconductivity in a Cu-doped lead-apatite (LK-99) has ignited substantial research interest in both experimental and theoretical domains. Previous density functional theory (DFT) calculations with the inclusion of an on-site Hubbard interaction U consistently predict the presence of flat bands crossing the Fermi level. This is in contrast to DFT plus dynamical mean-field theory (DMFT) calculations, which reveal the Mott insulating behavior for the stoichiometric $\text{Pb}_9\text{Cu}(\text{PO}_4)_6\text{O}$ compound. Nevertheless, the existing calculations are all based on the parent $P6_3/m$ - $\text{Pb}_{10}(\text{PO}_4)_6\text{O}$ structure, which is argued to be not the ground-state structure. Here, we revisit the electronic structure of $\text{Pb}_9\text{Cu}(\text{PO}_4)_6\text{O}$ with the energetically more favorable $P\bar{3}$ structure, fully taking into account electronic symmetry breaking. We examine all possible configurations for Cu substituting the Pb sites. Our results show that the doped Cu atoms exhibit a preference for substituting the Pb2 sites rather than the Pb1 sites. In both cases, the calculated substitutional formation energies are large, indicating the difficulty in incorporating Cu at the Pb sites. We find that most of the structures with Cu at the Pb2 site tend to be insulating, while the structures with both Cu atoms at the Pb1 sites (except one configuration) are predicted to be metallic by DFT + U calculations. However, when accounting for the electronic symmetry breaking, some Cu-doped configurations previously predicted to be metallic (including the structure studied in previous DFT + U calculations) become insulating. Our work highlights the importance of symmetry breaking in obtaining a correct electronic state for $\text{Pb}_9\text{Cu}(\text{PO}_4)_6\text{O}$, thereby reconciling previous DFT + U and DFT + DMFT calculations.

DOI: [10.1103/PhysRevB.108.L161101](https://doi.org/10.1103/PhysRevB.108.L161101)**I. INTRODUCTION**

Due to the potential for technological revolutions, the search for high- T_c superconductors under ambient conditions has persisted as a long-standing aspiration for both experimental and theoretical scientists. In light of this, the recent report claiming room-temperature ambient-pressure superconductivity and diamagnetism in a Cu-doped lead-apatite (LK-99) [1,2] has sparked substantial excitement not only within the physics community but also in the fields of chemistry and materials science. Several independent experimental groups have tried to synthesize LK-99 [3–19], but the claimed superconductivity of LK-99 has not been obtained. Notably, the experimentally observed sudden decrease in resistivity at approximately 400 K was argued to be attributed to a first-order transition from the high-temperature insulating β - Cu_2S phase to the low-temperature semiconducting γ - Cu_2S phase [9–11], and the half levitation observed in experiments was explained by the presence of soft ferromagnetism [6]. Moreover, insulating transport behaviors were observed by several experimental groups in their synthesized samples [14–19]. In contrast, density functional theory (DFT) calculations [20–31] and model Hamiltonian calculations [32–34] consistently pre-

dicted the presence of flat bands crossing the Fermi level due to the spatial separation of Cu atoms. DFT plus dynamical mean-field theory (DFT + DMFT) calculations [26–28], however, demonstrated that the stoichiometric $\text{Pb}_9\text{Cu}(\text{PO}_4)_6\text{O}$ compound is actually a Mott insulator due to the very large interaction versus bandwidth ratio $U/W > 30$ and additional electron doping is needed to achieve a conducting state. The calculations using the fluctuation exchange method showed that spin and orbital fluctuations are too weak even under optimized conditions for superconductivity, indicating the absence of superconductivity in $\text{Pb}_9\text{Cu}(\text{PO}_4)_6\text{O}$ [31].

It is important to note that the existing calculations are all based on the $P6_3/m$ - $\text{Pb}_{10}(\text{PO}_4)_6\text{O}$ (space group No. 176) structure as refined by Krivovichev and Burns in 2003 [35]. Very recently, Krivovichev and Engel [36] reinvestigated the crystal structure of $\text{Pb}_{10}(\text{PO}_4)_6\text{O}$ by single-crystal x-ray diffraction (XRD) using crystals prepared by Merker and Wondratschek [37] and concluded that the ground-state structure of $\text{Pb}_{10}(\text{PO}_4)_6\text{O}$ is a superstructure with the c lattice parameter doubled with respect to the $P6_3/m$ structure and exhibits a $P\bar{3}$ (space group No. 147) symmetry [36]. According to the analysis of Krivovichev and Engel [36], the $P6_3/m$ - $\text{Pb}_{10}(\text{PO}_4)_6\text{O}$ structure may correspond to the $\text{Pb}_{10}(\text{PO}_4)_6\text{O}_x(\text{OH})_{2-x}$ ($x \sim 0.4$) member of the $\text{Pb}_{10}(\text{PO}_4)_6\text{O}$ - $\text{Pb}_{10}(\text{PO}_4)_6(\text{OH})_2$ solid solution series, or to the high-temperature polymorph of $\text{Pb}_{10}(\text{PO}_4)_6\text{O}$ [36]. This important finding therefore raises a critical question of whether the conclusions drawn from previous calculations relying on

*These authors contributed equally to this work.

†jxli15s@imr.ac.cn

‡ptliu@imr.ac.cn

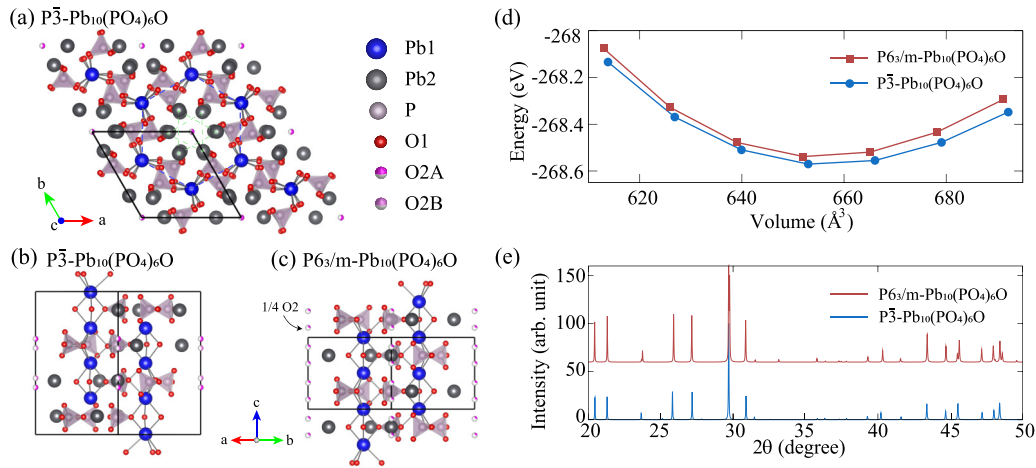


FIG. 1. (a) Top view of the crystal structure of $P\bar{3}$ - $Pb_{10}(PO_4)_6O$. (b) Side view of the crystal structure of $P\bar{3}$ - $Pb_{10}(PO_4)_6O$. (c) Side view of the crystal structure of $P6_3/m$ - $Pb_{10}(PO_4)_6O$. The black lines in (a)–(c) indicate the unit cell that is periodically replicated. (d) Energy-volume curves. Note that for a direct comparison, the total energy and volume of the $P6_3/m$ structure are doubled. (e) Simulated XRD patterns.

the high-temperature $P6_3/m$ - $Pb_{10}(PO_4)_6O$ structure remain valid when using the proposed ground-state $P\bar{3}$ - $Pb_{10}(PO_4)_6O$ structure.

In this work, we revisit the electronic structure of $Pb_9Cu(PO_4)_6O$ with the proposed $P\bar{3}$ ground-state structure using the DFT + U method and the DFT + DMFT approach, fully accounting for electronic symmetry breaking (ESB). We find that the newly refined $P\bar{3}$ - $Pb_{10}(PO_4)_6O$ superstructure is also an insulator, but energetically more favorable than the $P6_3/m$ structure. Both structures are found to be dynamically unstable due to the partial site occupancy of “extra” O atoms. Regarding the Cu-doped case, we examine all possible configurations for Cu substituting the Pb sites, leading to in total 44 symmetry-inequivalent configurations. Our results show that the doped Cu atoms prefer to substitute the Pb2 sites rather than the Pb1 sites that previous calculations assumed in their employed structures [see Fig. 1(a) for positions of Pb1 and Pb2 atoms]. In both cases, the calculated substitutional formation energies are large. The structures with Cu at the Pb2 sites tend to be insulating. In contrast, the structures with both Cu atoms at the Pb1 sites (except one configuration) are predicted to be metallic by DFT + U . However, the band gap is opened for some Cu-doped configurations when the ESB is taken into account. We note that our finding also applies to the Cu-doped $P6_3/m$ - $Pb_{10}(PO_4)_6O$ studied in previous DFT + U calculations [20–24,27]. This work stresses the importance of symmetry breaking in obtaining a correct insulating electronic state for $Pb_9Cu(PO_4)_6O$, and therefore, reconciles previous DFT + U and DFT + DMFT calculations.

II. COMPUTATIONAL DETAILS

For all the DFT + U calculations, we utilized computational settings similar to those employed in our previous work [20]. Specifically, the Vienna *ab initio* simulation package (VASP) [38,39] was used. The plane-wave cutoff was chosen to be 520 eV. A Γ -centered k -point grid with a k spacing of $0.03 \text{ } 2\pi/\text{\AA}$ (corresponding to a $4 \times 4 \times 2$ k -point grid) was used for structural relaxations and the k spacing was reduced to $0.02 \text{ } 2\pi/\text{\AA}$ (corresponding to a $9 \times 9 \times 3$ k -point

grid) for more accurate total energy and electronic structure calculations. The electronic interactions were described using the Perdew-Burke-Ernzerhof (PBE) functional [40]. The VASP recommended projector augmented wave pseudopotentials [41,42] were employed. The tetrahedron method with Blöchl corrections was used for density of states (DOSs) calculations, whereas the Gaussian smearing method with a smearing width of 0.05 eV was used for other calculations. The convergence criteria for the total energy and ionic forces were set to 10^{-6} eV and 0.01 eV/\AA , respectively. The phonon dispersions were calculated by finite displacements using the PHONOPY code [43]. For phonon calculations, a $2 \times 2 \times 2$ supercell [656 and 328 atoms for $P\bar{3}$ - and $P6_3/m$ - $Pb_{10}(PO_4)_6O$ structures, respectively] was used and the k -point grid was reduced to the Γ point only. The static electronic correlation effects were described using Dudarev’s DFT + U scheme [44,45] with the Hubbard interaction $U = 4 \text{ eV}$ [46] on the Cu $3d$ shell.

To study the effect of dynamical electronic correlation effects, we also conducted DFT + DMFT calculations [47,48]. For the DFT part, the all-electron WIEN2K package [49] was employed. The adopted atomic spheres R_{MT} were 2.13, 2.35, 1.53, and 1.39 bohr for Cu, Pb, P, and O, respectively, and the plane-wave cutoff K_{max} was set to $R_{MT}K_{max} = 7.0$. The impurity problem in the DMFT calculation was solved by the continuous time quantum Monte Carlo method [50,51] at a temperature of 387 K. The spectral functions along the real-frequency axis were obtained by analytical continuation using the maximum entropy method [48].

III. STRUCTURAL, ELECTRONIC, AND DYNAMICAL PROPERTIES OF LEAD-APATITE

Figures 1(a) and 1(c) compare the crystal structures of $P\bar{3}$ - and $P6_3/m$ - $Pb_{10}(PO_4)_6O$. In both structures, there exist two symmetry-inequivalent Pb atoms, named Pb1 and Pb2. The Pb1 atoms form a hexagon, whereas the Pb2 atoms form two oppositely shaped triangles [see Fig. 1(a)]. Along the c axis, the Pb2 atoms along with the surrounding insulating PO_4 units form a cylindrical column centered at “extra” O2 atoms [Fig. 1(a)]. The noticeable difference between the two

TABLE I. DFT-predicted lattice parameters a and c (in Å), and volume (in Å³) of $\text{Pb}_{10}(\text{PO}_4)_6\text{O}$ with $P6_3/m$ or $P\bar{3}$ symmetries. The available experimental data are given for comparison.

	a	c	Volume
$P6_3/m$ - $\text{Pb}_{10}(\text{PO}_4)_6\text{O}$ (Calc.)	10.024	7.482	651.02
$P6_3/m$ - $\text{Pb}_{10}(\text{PO}_4)_6\text{O}$ (Expt.) [35]	9.865	7.431	626.25
$P\bar{3}$ - $\text{Pb}_{10}(\text{PO}_4)_6\text{O}$ (Calc.)	10.019	15.034	1306.80
$P\bar{3}$ - $\text{Pb}_{10}(\text{PO}_4)_6\text{O}$ (Expt.) [36]	9.811	14.840	1237.06

structures lies in the doubling of the c lattice parameter in $P\bar{3}$ - $\text{Pb}_{10}(\text{PO}_4)_6\text{O}$ [compare Figs. 1(b) and 1(c)]. This is caused by the ordering of the O2 atoms within the structure channels along the c axis [36]. The O2 atoms form short bonds to the Pb2 atoms, leading to two different sites Pb2A and Pb2B. We note that for the $P6_3/m$ structure, the O2 atoms are 0.25 occupied [35], while for the $P\bar{3}$ structure, the O2A atoms are 0.55 occupied and O2B atoms are 0.45 occupied [36]. To model these structures, we removed three out of four O2 atoms for the $P6_3/m$ structure, whereas for the $P\bar{3}$ structure only the O2B atoms were kept. The calculated lattice parameters of both structures are compiled in Table I, showing good agreement with respective experimental values [35,36]. The overestimated predicted lattice parameters are due to the employed PBE functional. The structural data of $P\bar{3}$ - and $P6_3/m$ - $\text{Pb}_{10}(\text{PO}_4)_6\text{O}$ are provided in the Supplemental Material [52]. The calculated energy-volume curves for both $P\bar{3}$ - and $P6_3/m$ - $\text{Pb}_{10}(\text{PO}_4)_6\text{O}$ are shown in Fig. 1(d). It is evident that the $P\bar{3}$ structure is energetically more favorable than the $P6_3/m$ structure across the entire range of volumes considered. However, both structures display similar XRD

patterns that are difficult to visually differentiate. Upon closer examination, one can see that the $P\bar{3}$ structure exhibits additional minor peaks at around 25, 28, 45.5, 48, and 48.5 degrees.

Furthermore, we conducted phonon calculations and found that both structures are dynamically unstable at the harmonic level [see Figs. 2(a) and 2(d)]. The calculated phonon DOSs indicate that the imaginary phonon modes for both structures arise from the partial site occupancy of “extra” O2 atoms and associated neighboring Pb atoms [see Figs. 2(b) and 2(e)]. Our calculated phonon instability of $P6_3/m$ - $\text{Pb}_{10}(\text{PO}_4)_6\text{O}$ is consistent with previous DFT results [30,53]. Turning to the electronic structure, we found that similar to the $P6_3/m$ compound, the $P\bar{3}$ - $\text{Pb}_{10}(\text{PO}_4)_6\text{O}$ compound is also a nonmagnetic insulator, with a PBE-predicted indirect gap of 2.96 eV [compare Figs. 2(c) and 2(f)]. The obtained insulating nature of lead-apatite is consistent with the experimental observation [2].

IV. ELECTRONIC STRUCTURE OF COPPER-DOPED LEAD-APATITE

Having identified the ground-state structure of $\text{Pb}_{10}(\text{PO}_4)_6\text{O}$, we now shift our focus to the Cu-doped case. According to experiment [2], the LK-99 possesses a chemical formula of $\text{Pb}_{10-x}\text{Cu}_x(\text{PO}_4)_6\text{O}$ ($0.9 < x < 1.1$) with the Cu atoms substituting the Pb1 positions [2]. For simplicity, here we considered $x = 1$, which was obtained by substituting two Pb atoms with two Cu atoms in the $P\bar{3}$ - $\text{Pb}_{10}(\text{PO}_4)_6\text{O}$ superstructure. We examined all possible configurations for Cu substituting the Pb sites. Eventually, 44 symmetry-inequivalent configurations were obtained (see Supplemental Material Fig. S1 [52]). The computed

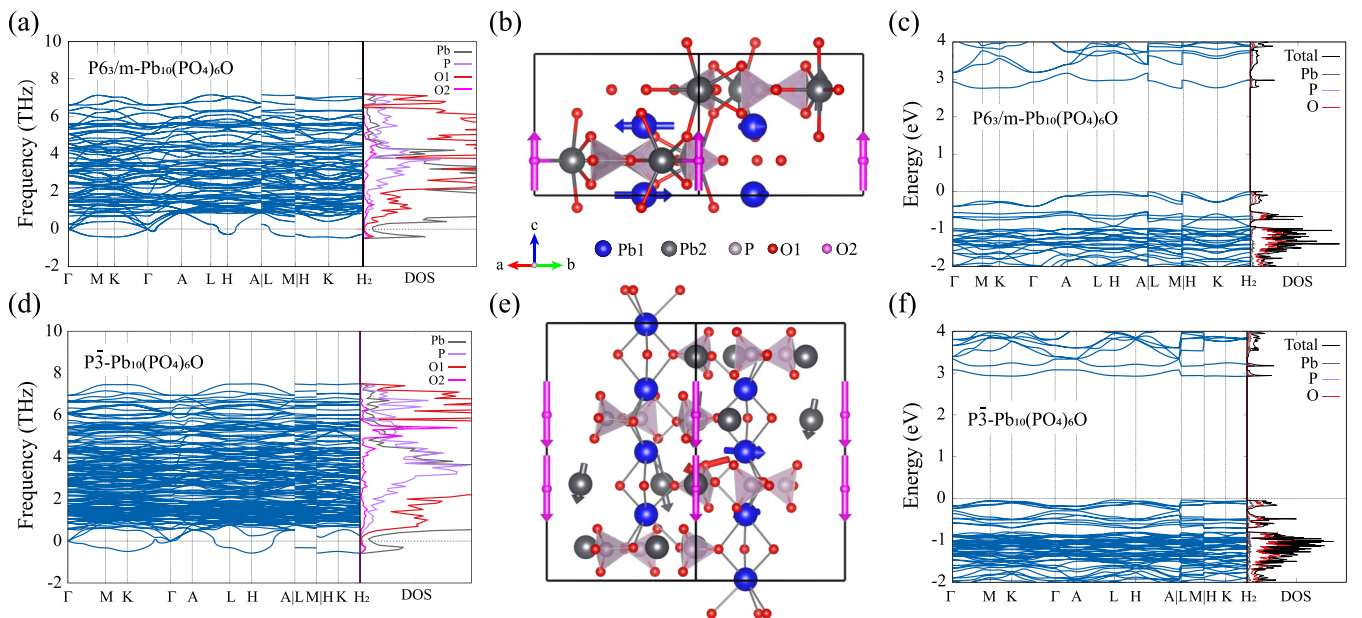


FIG. 2. Calculated phonon dispersions and DOSs (first column), atomic displacements (in arrows) associated with the imaginary frequency at M (0.5, 0, 0) point (middle column), and electronic band structure and DOSs (last column) for (a)-(c) $P6_3/m$ - $\text{Pb}_{10}(\text{PO}_4)_6\text{O}$ and (d)-(f) $P\bar{3}$ - $\text{Pb}_{10}(\text{PO}_4)_6\text{O}$. Note that for a better visualization of the phonon branches with imaginary frequencies, the phonon frequencies beyond 10 THz are not shown.

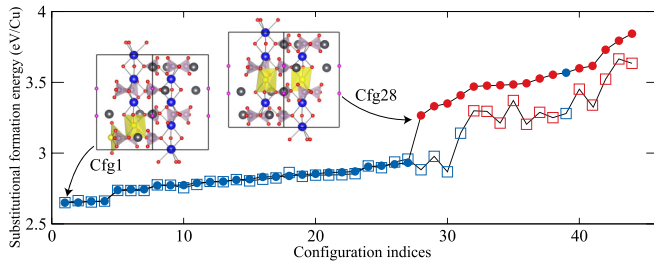


FIG. 3. Computed Cu \rightarrow Pb substitutional formation energies (E_f) for 44 symmetry-inequivalent configurations. The configurations are arranged in ascending E_f calculated by magnetically collinear DFT + U without ESB (in circles), and their crystal structures are shown in Supplemental Material Fig. S1 [52]. The DFT + U + SOC calculated E_f are displayed in squares. The blue and red colors indicate the insulating and metallic states, respectively. We note that the configuration Cfg39 is found to be a robust FM insulator, regardless of ESB or variation of U . All the data associated with this plot are provided in Supplemental Material Table S1 [52].

substitutional formation energies for all the configurations are displayed in Fig. 3. We note that in our formation energy calculations, we did not consider the possible secondary phases that can restrict the chemical potentials of involved species [54] and the calculated values should correspond to the Pb-rich condition. Therefore, a direct comparison with experiment should be cautious.

Let us begin by examining the general trend revealed by these magnetically collinear DFT + U (without ESB) data, and then delve into a detailed discussion about the specific configurations. First, one can see that the substitutional formation energies are overall large. The lowest-energy configuration (Cfg1) with one Cu atom at a Pb2 site and the other Cu atom at the neighboring Pb1 site is insulating (see Supplemental Material Fig. S2 [52]) and exhibits a substitutional formation energy of 2.65 eV/Cu. These results indicate the difficulty in incorporating Cu atoms at the Pb sites, in line with experimental implications [13]. In general, the doped Cu atoms exhibit a preference for substituting the Pb2 sites rather than the Pb1 sites, which is manifested by overall larger substitutional formation energies for the configurations with two Cu atoms at the Pb1 sites (except Cfg30) than those configurations with at least one Cu atom at the Pb2 site (see Fig. 3 and Supplemental Material Fig. S1 [52]). Additionally, an interesting observation is that the two Cu atoms have a tendency to approach each other, indicating a preference for Cu-Cu interactions or clustering within the lattice. Second, it can be seen that the energetically more favorable configurations are mostly insulating. The abrupt increase appearing in DFT + U calculated substitutional formation energies corresponds to the boundary between insulators and metals. Third, for the configurations where both Cu atoms are at the Pb1 sites, the configuration Cfg28 is found to exhibit the lowest substitutional formation energy. In this structure, the two Cu atoms form a hexagonal lattice in the ab plane and are related to each other by inversion symmetry, thereby preserving the $P\bar{3}$ symmetry of the system. The magnetically collinear DFT + U calculations without ESB predict Cfg28 to be metallic, with four spin-polarized flat bands around the Fermi level, similar

to what was observed for the $P6_3/m$ - $Pb_9Cu(PO_4)_6O$ structure in previous DFT + U calculations [20–24,27]. Under the time-reversal symmetry breaking, two Weyl points can be observed at high-symmetry points K and H [see Fig. 4(a)].

It should be noted that the long-range ferromagnetic (FM) ordering was adopted for the above DFT + U calculations. Despite being lower in energy as compared to the antiferromagnetic and nonmagnetic configurations, the FM ordered configuration without ESB may trap in a high-symmetry local energy minima. To check this point, we performed electronic optimization with the ESB accounted for. This is achieved by switching off the symmetry and using the conjugate gradient algorithm [55] during the electronic optimization. Interestingly, with the ESB, the band gap is opened, leading to an insulating state [compare Figs. 4(b) and 4(a)]. Meanwhile, the total energy is significantly lowered by 0.57 eV per unit cell. In addition, we also conducted magnetically noncollinear DFT + U calculations with the ESB, yielding a similar insulating band structure [compare Figs. 4(c) and 4(b)] and a decreased system energy (see Fig. 3). The effect of spin-orbit coupling (SOC) was also investigated, and as expected, the SOC exhibits negligible effect [compare Figs. 4(c) and 4(d)]. Furthermore, we also reexamined the electronic structure of $P6_3/m$ - $Pb_9Cu(PO_4)_6O$. We recall that the $P6_3/m$ structure is the one that was studied by previous calculations in literature [20–34]. For this structure, the Cu atom is placed at the energetically unfavorable Pb1 site. Previous magnetically collinear DFT + U calculations without the ESB predicted a metallic state with two flat bands around the Fermi level. However, with the ESB, the band gap is also opened (see Supplemental Material Fig. S3 [52]). All these results suggest that the previously reported flat-band metallic state is a result of an artifact of DFT + U calculations without considering the ESB. As a complement to our work, Swift and Lyons [56] recently commented that the incorrect prediction by DFT + U calculations originates from the overestimation of the energy of the O-2 p states in the valence band. This can be remedied by hybrid functional calculations [56] or quasiparticle self-consistent GW calculations [57]. We note that similar situations apply to the configurations Cfg29, Cfg30, and Cfg31, for which noncollinear DFT + U calculations with the ESB also result in gap opening (see Fig. 3). We also checked the U dependence and found that the smaller value of $U = 3.0$ eV does not change the conclusion.

Before closing this section, we would like to briefly discuss the effect of dynamical electronic correlations. As introduced in the Introduction, DFT + DMFT calculations [26–28] showed that the stoichiometric $Pb_9Cu(PO_4)_6O$ compound is a Mott insulator. Again, the employed structure relies on the $P6_3/m$ structure with the Cu atom at the Pb1 site. Here, we conducted paramagnetic DFT + DMFT calculations at 387 K for the Cfg28- $P\bar{3}$ - $Pb_9Cu(PO_4)_6O$ structure. The local interactions were treated at the density-density level, with the Hund's coupling $J = 0.07U$ and $U = 7.0$ eV. The large U value used here is due to the fact that we employed a full-potential DMFT implementation [48] that incorporates the states spanning a large energy window around the Fermi level. These interaction parameters are comparable to cuprates ($U = 7.0$ eV within the d - p model [58]) and also to $P6_3/m$ - $Pb_9Cu(PO_4)_6O$ ($U = 5.67$ eV within the d - p model [28]). The DFT + DMFT

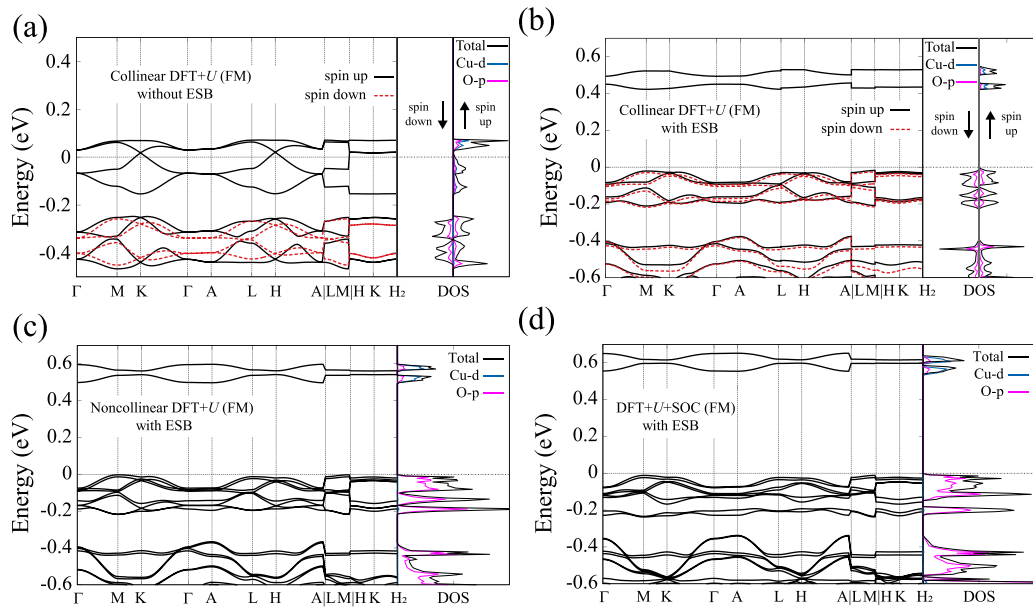


FIG. 4. Predicted electronic band structures and density of states for Cfg28- $P\bar{3}$ -Pb₉Cu(PO₄)₆O by (a) magnetically collinear DFT + U without ESB, (b) magnetically collinear DFT + U with ESB, (c) magnetically noncollinear DFT + U with ESB, and (d) DFT + U + SOC with ESB. A ferromagnetic setup is adopted for all the calculations.

calculated DOSs for Cfg28- $P\bar{3}$ -Pb₉Cu(PO₄)₆O are displayed in Fig. 5. It can be seen that, in contrast to the prediction by the magnetically collinear DFT + U without ESB, the paramagnetic DFT + DMFT predicts an insulating state for the Cfg28- $P\bar{3}$ -Pb₉Cu(PO₄)₆O compound, similar to the $P6_3/m$ -Pb₉Cu(PO₄)₆O compound [26–28]. All these results conclude that the stoichiometric Cfg28- $P\bar{3}$ -Pb₉Cu(PO₄)₆O structure is a robust insulator at both low and high temperatures.

V. CONCLUSIONS

In conclusion, we have revisited the electronic structure of Pb₉Cu(PO₄)₆O based on the energetically more favorable $P\bar{3}$ -Pb₁₀(PO₄)₆O structure, fully taking into account the ESB. We examine all possible configurations for Cu substituting the Pb sites and demonstrate that the doped Cu atoms exhibit a preference for substituting the Pb2 sites rather than the Pb1 sites. In both cases, the calculated substitutional formation energies are large, posing a great challenge for experiments to dope Cu atoms at the Pb sites. It is found that the energetically favorable Cu-doped configurations are insu-

lating, in line with many experimental observations showing insulating transport behaviors in synthesized samples [14–19]. Our calculations show that the conducting state can only be obtained in a few Cu-doped configurations with Cu atoms at the Pb1 sites. However, due to their overall larger substitutional formation energies, it would be difficult to obtain a conducting state for stoichiometric Pb₉Cu(PO₄)₆O just by doping Cu atoms from a thermodynamical perspective. Importantly, we find that the magnetically collinear DFT + U method without the electronic symmetry breaking predicts an incorrect flat-band metallic state for some Cu-doped configurations with Cu atoms at the Pb1 sites. These also include the $P6_3/m$ -Pb₉Cu(PO₄)₆O structure that previous DFT + U calculations rely on. By accounting for the ESB, the correct insulating electronic state is obtained. This has been demonstrated by simply incorporating the ESB in magnetically collinear DFT + U calculations, or through magnetically noncollinear DFT + U calculations and DFT + DMFT calculations. Our work emphasizes the importance of symmetry breaking in electronic structure calculations and reconciles the inconsistency between previous DFT + U and DFT + DMFT calculations.

Note added. We recently became aware of other independent studies that also emphasize the importance of symmetry breaking [59,60].

ACKNOWLEDGMENTS

The authors thank Dr. S. V. Krivovichev for sharing the structural data of $P\bar{3}$ -Pb₁₀(PO₄)₆O. This work was supported by the National Natural Science Foundation of China (Grant No. 52201030). J.L. acknowledges the funding from China Postdoctoral Science Foundation (Grants No. 2022T150660 and No. 2021M700152).

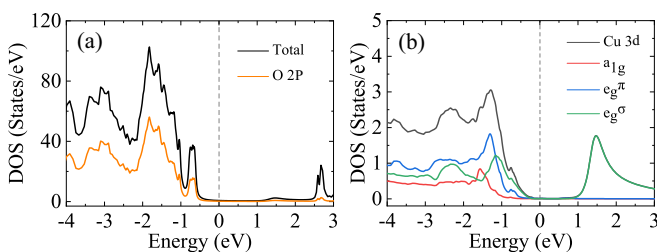


FIG. 5. DFT + DMFT calculated density of states for Cfg28- $P\bar{3}$ -Pb₉Cu(PO₄)₆O at 387 K. A paramagnetic setup is adopted.

- [1] S. Lee, J.-H. Kim, and Y.-W. Kwon, [arXiv:2307.12008](https://arxiv.org/abs/2307.12008).
- [2] S. Lee, J. Kim, H.-T. Kim, S. Im, S. An, and K. H. Auh, [arXiv:2307.12037](https://arxiv.org/abs/2307.12037).
- [3] L. Liu, Z. Meng, X. Wang, H. Chen, Z. Duan, X. Zhou, H. Yan, P. Qin, and Z. Liu, *Adv. Funct. Mater.* **2308938** (2023).
- [4] H. Wu, L. Yang, B. Xiao, and H. Chang, [arXiv:2308.01516](https://arxiv.org/abs/2308.01516).
- [5] P. Abramian, A. Kuzanyan, V. Nikoghosyan, S. Teknowijoyo, and A. Gulian, [arXiv:2308.01723](https://arxiv.org/abs/2308.01723).
- [6] K. Guo, Y. Li, and S. Jia, *Sci. China: Phys., Mech. Astron.* **66**, 107411 (2023).
- [7] K. Kumar, N. K. Karn, Y. Kumar, and V. P. S. Awana, [arXiv:2308.03544](https://arxiv.org/abs/2308.03544).
- [8] I. Timokhin, C. Chen, Q. Yang, and A. Mishchenko, [arXiv:2308.03823](https://arxiv.org/abs/2308.03823).
- [9] S. Zhu, W. Wu, Z. Li, and J. Luo, [arXiv:2308.04353](https://arxiv.org/abs/2308.04353).
- [10] P. K. Jain, *J. Phys. Chem. C* **127**, 18253 (2023).
- [11] C. Liu, W. Cheng, X. Zhang, J. Xu, J. Li, Q. Shi, C. Yuan, L. Xu, H. Zhou, S. Zhu, J. Sun, W. Wu, J. Luo, K. Jin, and Y. Li, *Phys. Rev. Mater.* **7**, 084804 (2023).
- [12] H. Wu, L. Yang, J. Yu, G. Zhang, B. Xiao, and H. Chang, [arXiv:2308.05001](https://arxiv.org/abs/2308.05001).
- [13] G. S. Thakur, M. Schulze, and M. Ruck, [arXiv:2308.05776](https://arxiv.org/abs/2308.05776).
- [14] K. Kumar, N. K. Karn, and V. P. S. Awana, *Supercond. Sci. Technol.* **36**, 10LT02 (2023).
- [15] Y. Zhang, C. Liu, X. Zhu, and H.-H. Wen, [arXiv:2308.05786](https://arxiv.org/abs/2308.05786).
- [16] P. Puphal, M. Y. P. Akbar, M. Hepting, E. Goering, M. Isobe, A. A. Nugroho, and B. Keimer, [arXiv:2308.06256](https://arxiv.org/abs/2308.06256).
- [17] Q. Hou, W. Wei, X. Zhou, X. Wang, Y. Sun, and Z. Shi, [arXiv:2308.05778](https://arxiv.org/abs/2308.05778).
- [18] H. Singh, A. Gautam, M. Singh, P. Saha, P. Kumar, P. Das, M. Lamba, K. Yadav, P. K. Mishra, S. Patnaik, and A. Ganguli, [arXiv:2308.06589](https://arxiv.org/abs/2308.06589).
- [19] P. Wang, X. Liu, J. Ge, C. Ji, H. Ji, Y. Liu, Y. Ai, G. Ma, S. Qi, and J. Wang, *Quantum Front.* **2**, 10 (2023).
- [20] J. Lai, J. Li, P. Liu, Y. Sun, and X.-Q. Chen, *J. Mater. Sci. Technol.* **171**, 66 (2024).
- [21] S. M. Griffin, [arXiv:2307.16892](https://arxiv.org/abs/2307.16892).
- [22] L. Si and K. Held, *Phys. Rev. B* **108**, L121110 (2023).
- [23] R. Kurlito, S. Lany, D. Pashov, S. Acharya, M. van Schilfgaarde, and D. S. Dessau, [arXiv:2308.00698](https://arxiv.org/abs/2308.00698).
- [24] J. Cabezas-Escases, N. F. Barrera, C. Cardenas, and F. Munoz, [arXiv:2308.01135](https://arxiv.org/abs/2308.01135).
- [25] K. Tao, R. Chen, L. Yang, J. Gao, D. Xue, and C. Jia, [arXiv:2308.03218](https://arxiv.org/abs/2308.03218).
- [26] D. M. Korotin, D. Y. Novoselov, A. O. Shorikov, V. I. Anisimov, and A. R. Oganov, [arXiv:2308.04301](https://arxiv.org/abs/2308.04301).
- [27] L. Si, M. Wallerberger, A. Smolyanyuk, S. di Cataldo, J. M. Tomczak, and K. Held, [arXiv:2308.04427](https://arxiv.org/abs/2308.04427).
- [28] C. Yue, V. Christiansson, and P. Werner, [arXiv:2308.04976](https://arxiv.org/abs/2308.04976).
- [29] Y. Jiang, S. B. Lee, J. Herzog-Arbeitman, J. Yu, X. Feng, H. Hu, D. Călugăru, P. S. Brodale, E. L. Gormley, M. G. Vergniory, C. Felser, S. Blanco-Canosa, C. H. Hendon, L. M. Schoop, and B. A. Bernevig, [arXiv:2308.05143](https://arxiv.org/abs/2308.05143).
- [30] L. Hao and E. Fu, [arXiv:2308.05618](https://arxiv.org/abs/2308.05618).
- [31] N. Witt, L. Si, J. M. Tomczak, K. Held, and T. Wehling, [arXiv:2308.07261](https://arxiv.org/abs/2308.07261).
- [32] O. Tavakol and T. Scaffidi, [arXiv:2308.01315](https://arxiv.org/abs/2308.01315).
- [33] H. Oh and Y.-H. Zhang, [arXiv:2308.02469](https://arxiv.org/abs/2308.02469).
- [34] W. Chen, [arXiv:2308.05124](https://arxiv.org/abs/2308.05124).
- [35] S. V. Krivovichev and P. C. Burns, *Z. Kristall. - Cryst. Mater.* **218**, 357 (2003).
- [36] S. V. Krivovichev and G. Engel, *Crystals* **13**, 1371 (2023).
- [37] L. Merker and H. Wondratschek, *Z. Anorg. Allg. Chem.* **306**, 25 (1960).
- [38] G. Kresse and J. Hafner, *Phys. Rev. B* **47**, 558 (1993).
- [39] G. Kresse and J. Furthmüller, *Phys. Rev. B* **54**, 11169 (1996).
- [40] J. P. Perdew, K. Burke, and M. Ernzerhof, *Phys. Rev. Lett.* **77**, 3865 (1996).
- [41] P. E. Blöchl, *Phys. Rev. B* **50**, 17953 (1994).
- [42] G. Kresse and D. Joubert, *Phys. Rev. B* **59**, 1758 (1999).
- [43] A. Togo and I. Tanaka, *Scr. Mater.* **108**, 1 (2015).
- [44] S. L. Dudarev, G. A. Botton, S. Y. Savrasov, C. J. Humphreys, and A. P. Sutton, *Phys. Rev. B* **57**, 1505 (1998).
- [45] S. L. Dudarev, P. Liu, D. A. Andersson, C. R. Stanek, T. Ozaki, and C. Franchini, *Phys. Rev. Mater.* **3**, 083802 (2019).
- [46] L. Wang, T. Maxisch, and G. Ceder, *Phys. Rev. B* **73**, 195107 (2006).
- [47] G. Kotliar, S. Y. Savrasov, K. Haule, V. S. Oudovenko, O. Parcollet, and C. A. Marianetti, *Rev. Mod. Phys.* **78**, 865 (2006).
- [48] K. Haule, C.-H. Yee, and K. Kim, *Phys. Rev. B* **81**, 195107 (2010).
- [49] P. Blaha, K. Schwarz, G. K. Madsen, D. Kvasnicka, J. Luitz *et al.*, *WIEN2k: An Augmented Plane Wave+Local Orbitals Program for Calculating Crystal Properties* (Techn. Universitat, 2019).
- [50] P. Werner, A. Comanac, L. de'Medic, M. Troyer, and A. J. Millis, *Phys. Rev. Lett.* **97**, 076405 (2006).
- [51] K. Haule, *Phys. Rev. B* **75**, 155113 (2007).
- [52] See Supplemental Material at <http://link.aps.org/supplemental/10.1103/PhysRevB.108.L161101> for the detailed information on employed structure models, different configurations of $P\bar{3}$ -Pb₉Cu(PO₄)₆O and their corresponding Cu → Pb substitutional formation energies, and the band structure of Cfg1- $P\bar{3}$ -Pb₁₀(PO₄)₆O.
- [53] J. Shen, D. G. II, S. Shahabfar, Z. Li, D. Kang, S. Griesemer, A. Salgado-Casanova, T.-C. Liu, C.-T. Chou, Y. Xia, and C. Wolverton, [arXiv:2308.07941](https://arxiv.org/abs/2308.07941).
- [54] C. Freysoldt, B. Grabowski, T. Hickel, J. Neugebauer, G. Kresse, A. Janotti, and C. G. Van de Walle, *Rev. Mod. Phys.* **86**, 253 (2014).
- [55] M. C. Payne, M. P. Teter, D. C. Allan, T. A. Arias, and J. D. Joannopoulos, *Rev. Mod. Phys.* **64**, 1045 (1992).
- [56] M. W. Swift and J. L. Lyons, [arXiv:2308.08458](https://arxiv.org/abs/2308.08458).
- [57] D. Pashov, S. Acharya, S. Lany, D. S. Dessau, and M. van Schilfgaarde, [arXiv:2308.09900](https://arxiv.org/abs/2308.09900).
- [58] P. Werner, R. Sakuma, F. Nilsson, and F. Aryasetiawan, *Phys. Rev. B* **91**, 125142 (2015).
- [59] A. B. Georgescu, [arXiv:2308.07295](https://arxiv.org/abs/2308.07295).
- [60] L. Celiberti, L. Varrassi, and C. Franchini, 2023, <https://www.researchgate.net/publication/373334869>.